

Improving High Resolution fMRI at 3T with the 32-Channel Head Array

Christina Triantafyllou^{1,2}; Lawrence L. Wald^{2,3}

¹Athinoula A. Martinos Imaging Center, McGovern Institute for Brain Research, Massachusetts Institute of Technology, Cambridge, MA, USA

²Athinoula A. Martinos Center for Biomedical Imaging, Department of Radiology, Massachusetts General Hospital, Boston, MA, USA

³Harvard-MIT Division of Health Sciences and Technology, Massachusetts Institute of Technology, Cambridge, MA, USA

Introduction

It is well known that BOLD (Blood Oxygenation Level Dependent) effects increase in amplitude at higher field strength, due to the general enhancement of susceptibility contrast resulting in improvements in BOLD sensitivity and specificity. Nevertheless, identifying additive methods of improving BOLD imaging are also worth pursuing. In particular, the new generation of highly parallel brain arrays offers a potential adjuvant approach to high field functional MRI (fMRI). These close-fitting, highly parallel detection arrays allow impressive increases in image signal-to-noise ratio (SNR) in cortical areas and increases in iPAT (integrated Parallel Acquisition Technique) acceleration, helpful for mitigating image distortion in EPI (Fig. 1) [1, 2]. It is nonetheless important to closely examine their benefits for fMRI, since the fMRI experiment is limited by physiological fluctuations in the time-series SNR (tSNR) rather than in the image SNR (SNR₀).

In this paper, we review our findings on the benefits of 32-channel receive arrays for the time-series SNR in the fMRI experiment and validate the sensitivity gains in two illustrative fMRI examples; retinotopy of the primary visual system and speech motor region activation. We show that highly parallel detection

offers a powerful adjuvant method to high field fMRI, especially when high resolution brain mapping is desired. The article is organized in two parts. First we characterize the fMRI time-series fluctuations (noise) for different coils and image resolution combinations as a metric for potential improvements in fMRI sensitivity. Second we show results from two real world fMRI experiments.

Physiological noise in fMRI time-series SNR using array coils

Our ability to detect small changes in image intensity associated with subtle brain activation in the fMRI time-series is limited by physiologically induced image intensity modulations (physiological noise). Thus, the noise in fMRI is not the traditional image noise important for anatomical imaging, but arises from the interplay between the imaging and physiological processes which occur during the time-series. The time-series SNR (tSNR) is the most important metric for determining the smallest activation effect which can be seen in a given fMRI experiment. It is defined as a pixel's mean intensity divided by the standard deviation of this intensity over time. In contrast, the image SNR (SNR₀) is defined as the image intensity divided by the noise in that image (traditionally taken as

the standard deviation in the image background area, although this definition is problematic for arrays).

Previous studies of the physiological noise in fMRI time-series have shown that it acts as a modulation of the image intensity with time [3, 4]. Thus, as the signal gets stronger (from higher field scanners or an improved head coil), then the physiological noise grows proportionally, since the noise level is a fixed percentage of the signal level. This is problematic in that at first glance it appears that improving detection sensitivity with array coils will not translate to improved tSNR for fMRI. Namely, gains in image sensitivity are offset by proportional gains in physiological noise. Defining σ_p as the physiological noise standard deviation, and S as the image signal intensity, Krüger and colleagues showed this scaling relationship; $\sigma_p = \lambda S$, where λ is a constant. But, the total time-series noise is the statistical sum of the physiological noise, σ_p , and the conventional image noise, σ_o , thus the potential benefit of improvements in array technology (which improves image SNR) will depend on the relative importance of these two noise sources. For example, as the voxel size is decreased, we expect thermal image noise to dominate and improvements in array technology will translate

to improved fMRI time-series SNR (tSNR). Thus, we sought to examine the benefits of high-N arrays on the tSNR in fMRI experiments of different image resolutions and using a range of head coils. At different image resolutions the time series noise can be expected to derive from varying ratios of physiological to image noise. Furthermore, since many fMRI studies now use iPAT to reduce the image distortion associated with single shot EPI, and since iPAT alters the image noise, we examine the effect of iPAT on fMRI time-series SNR by varying the degree of acceleration for a number of image resolutions commonly used in fMRI.

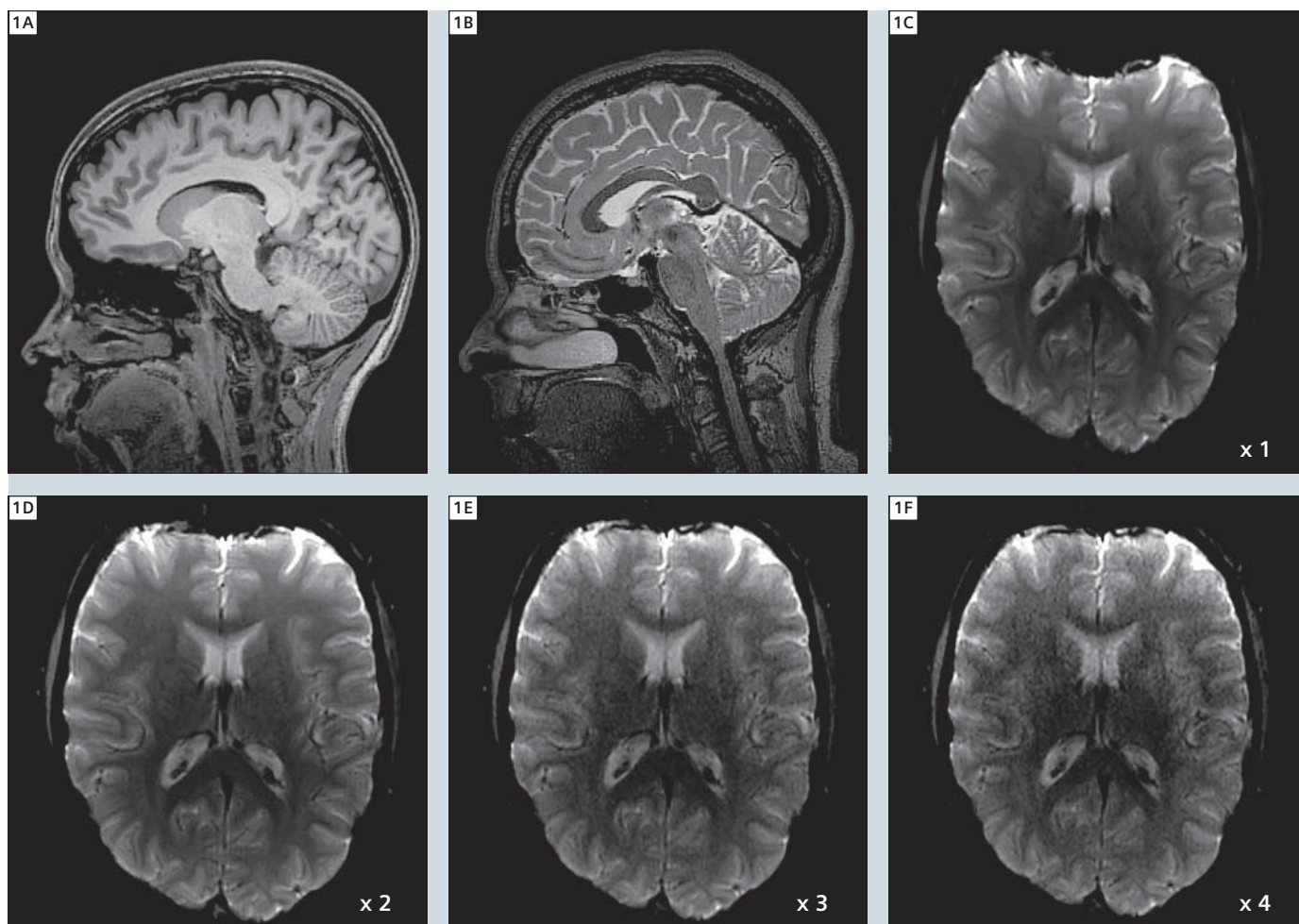
Methods

To evaluate the physiological noise in fMRI, resting state EPI time-series were collected at 3T on a MAGNETOM Trio, A Tim System, using a single-shot gradient echo EPI sequence and three different receive RF coils; a transmit/receive volume head coil (Birdcage), the 12-channel Matrix receive-only head coil, and the 32-channel receive-only phased array head coil. All subjects were asked to relax while in the scanner; no specific stimulus was applied. Written consent was obtained from all the subjects under protocols approved by institutional review. To achieve accurate comparison

between the coils, the same four healthy volunteers were scanned.

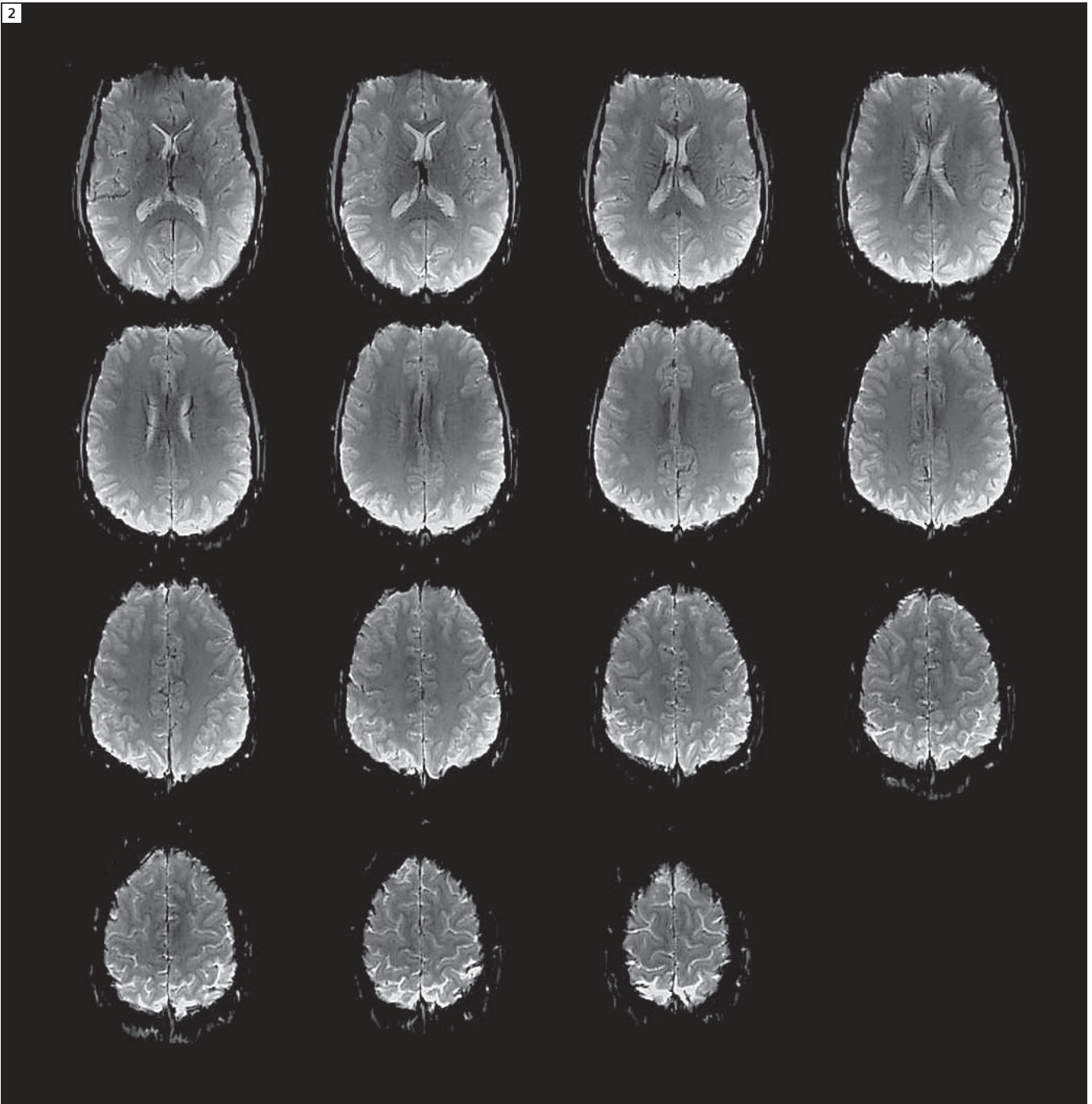
Data were collected parallel to the AC-PC line at six different in-plane resolutions ($1 \times 1 \text{ mm}^2$, $1.5 \times 1.5 \text{ mm}^2$, $2 \times 2 \text{ mm}^2$, $3 \times 3 \text{ mm}^2$, $4 \times 4 \text{ mm}^2$ and $5 \times 5 \text{ mm}^2$). Other imaging parameters were: slice thickness = 3 mm, TR = 5400 ms, TE = 30 ms, 60 time points, flip angle = 90° . Figure 2 shows example images from the $1 \times 1 \text{ mm}^2$ data set acquired with the 32-channel array.

The use of array data requires a more complex analysis to generate SNR_0 in a way that renders it directly comparable to time-series measurements [5]. After



1 High resolution images acquired with the 32-channel coil. **A:** T1-weighted 3D MPRAGE (1 mm isotropic). **B:** T2-weighted 3D-SPACE (0.6 mm isotropic). **C–F:** Single-shot gradient echo EPI images acquired at $1 \times 1 \times 3 \text{ mm}^3$, TE = 30 ms, with GRAPPA acceleration factors of 1–4, respectively (1 = no acceleration).

2



2 Resting state gradient echo 32-channel EPI images acquired at $1 \times 1 \times 3 \text{ mm}^3$ with $TE = 30 \text{ ms}$.

motion correction, time-series SNR maps (tSNR) were estimated as the ratio of the mean pixel intensity across time points to the temporal standard deviation. Measurements of tSNR and SNR_0 were evaluated in a cortical gray matter region-of-interest (ROI) and tSNR was

plotted as a function of SNR_0 for the different in-plane resolutions and receive coils. The data were fit to the model of Krüger et al. [3]. EPI time-series were also collected at three resolutions ($2 \times 2 \times 2 \text{ mm}^3$, $3 \times 3 \times 3 \text{ mm}^3$, $3 \times 3 \times 5 \text{ mm}^3$) using iPAT (*syngo* GRAPPA)

with acceleration factors of 1, 2, 3 and 4 at each resolution.

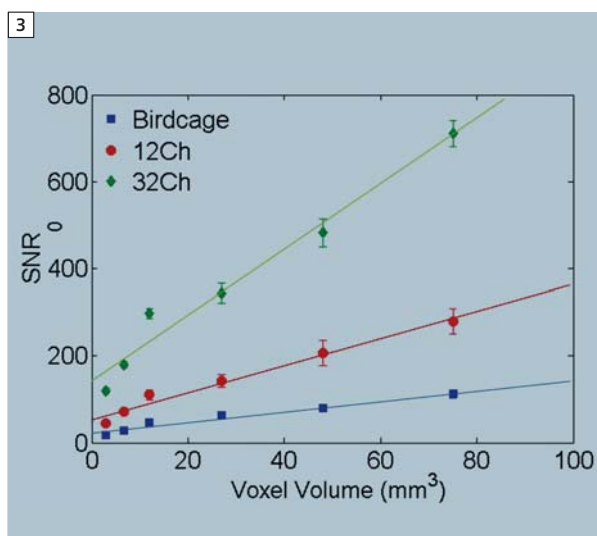
Results

Figure 3 shows SNR_0 as a function of voxel volume for the 3 different coils. As expected, the SNR_0 is nearly linear in

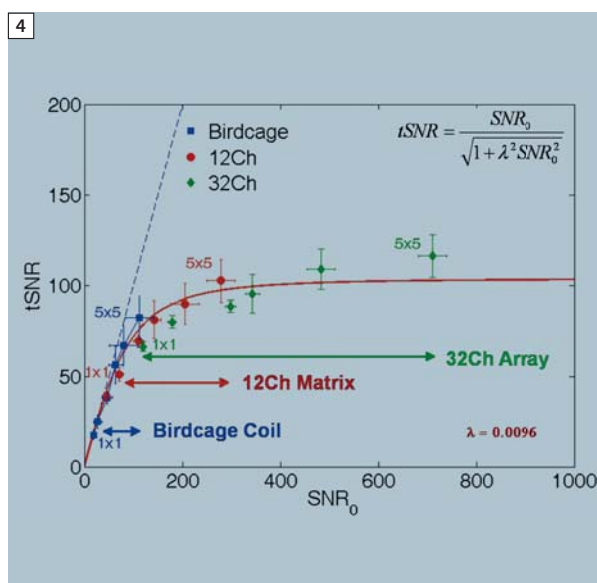
voxel volume and at each resolution the sensitivity is substantially improved in the cortex when the 32-channel array is used. For example, for the isotropic 3 mm voxel, the 32-channel SNR_0 was 1.2 fold higher than that of the 12-channel array. The results shown in Figure 4 suggest that the relationship between tSNR and SNR_0 can be well parameterized by the Krüger model at different resolutions and for array data. Namely, when SNR_0 is modulated by coil performance and image resolution, the physiological noise is well modeled as proportional to the signal. At low values of SNR_0 (small voxels or lower coil performance), the tSNR is dominated by thermal image noise and grows linearly with SNR_0 . As the image SNR increases (above approximately 200), then the curve approaches an asymptote and additional improvement in SNR_0 does not translate to substantial gains in tSNR. Since the highly parallel array coils chiefly increase image SNR, this suggests that their biggest benefits for fMRI (tSNR) will be for higher image resolutions where SNR_0 is below 200. For example, the 32-channel coil increased the tSNR of the $1.5 \times 1.5 \times 3 \text{ mm}^3$ acquisition by 57% compared to the 12-channel coil. At lower resolutions however, (e.g. $5 \times 5 \times 3 \text{ mm}^3$) the increase was only 13%.

Figure 5 shows the tSNR as a function of resolution at acceleration rates $R=1, 2, 3, 4$. The tSNR decreases at higher resolutions as expected, but is also reduced as R increases in all cases.

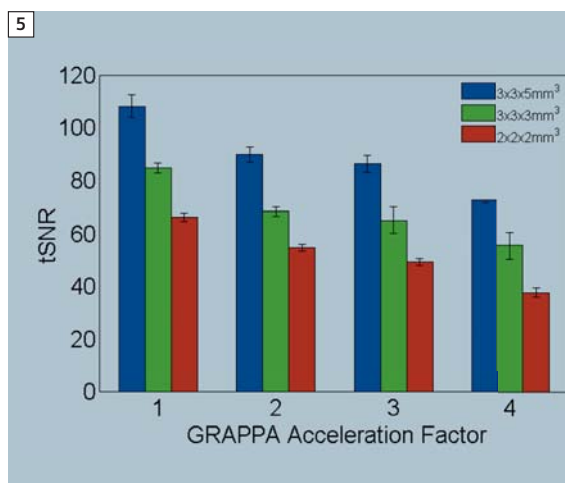
For example, at the lowest resolution used ($3 \times 3 \times 5 \text{ mm}^3$), tSNR decreased by 34% between the $R = 1$ and $R = 4$ acquisition showing that the improvement in susceptibility distortion afforded by iPAT comes at a cost in time-series SNR. For the higher resolution ($2 \times 2 \times 2 \text{ mm}^3$) the percentage decrease in tSNR between $R = 1$ to $R = 4$ is the greatest; 43%.



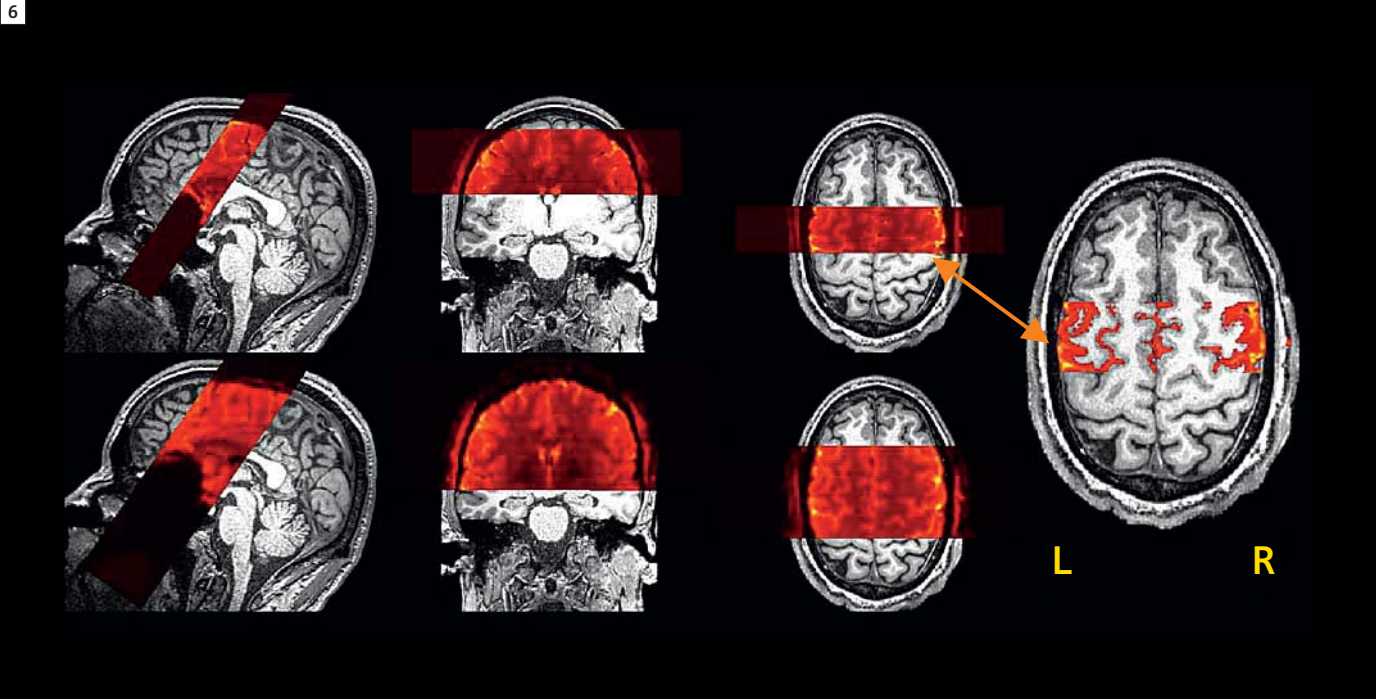
3 Image SNR (SNR_0) as a function of voxel volume. Lines are linear least-squares fit to the data.



4 SNR in fMRI time-series (tSNR) as a function of image SNR (SNR_0) for different spatial resolutions. Changes in image SNR were produced by varying the voxel volume and coils. Squares, circles and diamonds represent the 3T data for birdcage coil, 12-channel and the 32-channel array coil respectively. Measurements derived from areas of cortical gray matter and are averages over four subjects. The dotted line represents the line of identity ($tSNR = SNR_0$) which should parameterize the data in the absence of physiological noise, and the solid line shows the Krüger noise model fit to all the data points.



5 SNR in fMRI time-series (tSNR) as a function of acceleration factor at different spatial resolutions using the 32-channel coil. Measurements derived from areas of cortical gray matter and are averages over four subjects.



6 EPI slice prescription superimposed onto the high resolution 0.6 mm isotropic T1-weighted MPRAGE; top row 1 mm isotropic EPI data, bottom row 2 mm isotropic data, both acquired with 32-channel coil. Image on the right shows a thresholded EPI image and its correspondence to the T1-weighted anatomy. (Figure courtesy of S. Ghosh, MIT.)

Functional MRI applications

a) High-resolution fMRI using a 32-channel coil to identify individual-specific speech motor regions

Previous studies of overt speech sequencing [6] have reported activity in several brain regions such as ventral motor and pre-motor cortex, frontal operculum, posterior inferior frontal gyrus, supplementary motor area (SMA) and the pre-SMA. However, it has been difficult to reliably identify precise locations of activity in individuals because high spatial resolution is needed to resolve the ventral motor regions of the frontal lobe and the activation is weak for experiments limited to an individual. The spatial resolution problem is especially problematic for conventional resolutions ($3 \text{ mm}^2 \times 3 \text{ mm}^2$) and when spatial smoothing is needed in the statistical analysis. In this study, we will utilize the added sensitivity of the 32-channel coil to allow higher spatial resolution at acquisition in conjunction with reduced spatial smoothing

in the analysis, to allow the identification of the ventral motor regions in individual subjects and dissociate the clusters of activity around the frontal operculum and the supplementary motor area.

Methods

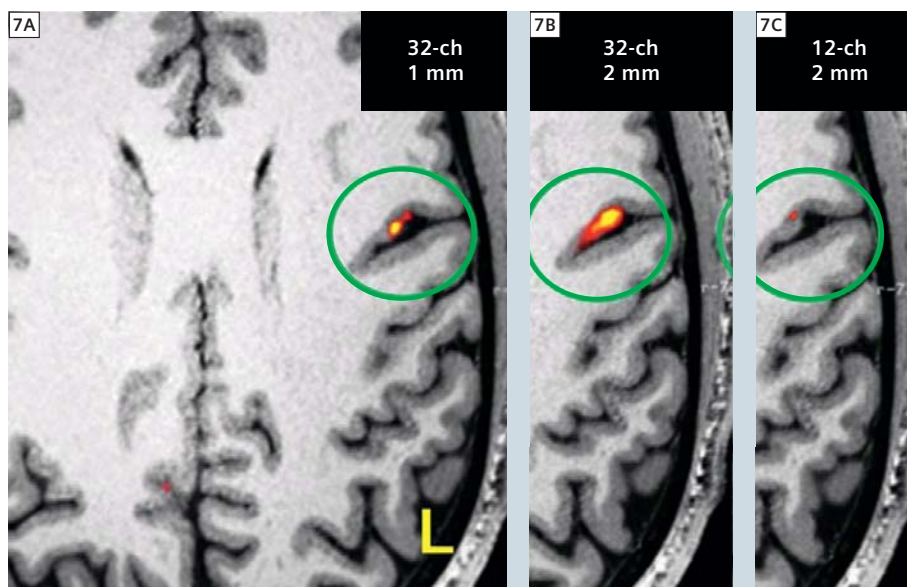
High-resolution single-shot gradient echo EPI time-series were acquired using the 32-channel phased array head coil. Written consent was obtained from all the subjects under protocols approved by institutional review. The imaging parameters were: TE = 30 ms, flip angle = 90° , TR = 12 s, TA = 2.5 s, TR delay = 9.5 s, *syngo* GRAPPA reconstruction with acceleration factor of 2. Twenty five 1 mm thick slices were acquired with an interslice gap of 0.1 mm, and in-plane resolutions of $1 \times 1 \text{ mm}^2$, FOV = 192×192 and matrix size = 192×192 . Slices were positioned so that they cover the SMA passing through the ventral pre-motor cortex (Fig. 6, top row). A second set of images with FOV = 256×256 and matrix size = 128×128 also acquired with in-plane resolution $2 \times 2 \text{ mm}^2$, and

slice thickness of 2 mm, (Fig. 6, bottom row). For comparison, 2 mm isotropic data was also acquired using the 12-channel Head Matrix coil. High resolution T1-weighted structural data was collected using an MPRAGE pulse sequence with isotropic voxel dimensions of 0.6 mm. Participants were asked to perform a speech task consisting of 3 conditions: **a)** speaking complex sequences of complex syllables (e.g., *stra-spli-stru*), **b)** speaking simple sequences of simple syllables (e.g., *ba-ba-ba*), and **c)** passively viewing the letter string (e.g., *xxx-xxx-xxx*) (baseline). Statistical analysis was performed using SPM5 (Wellcome Department of Cognitive Neurology, London, UK), including motion correction, smoothing and General Linear Model (GLM) fitting. The 1 mm and 2 mm data were smoothed with 2 mm and 4 mm FWHM Gaussian kernels respectively. Two contrasts were evaluated: **A)** speaking trials compared to baseline trials; and **B)** complex trials compared to simple trials.

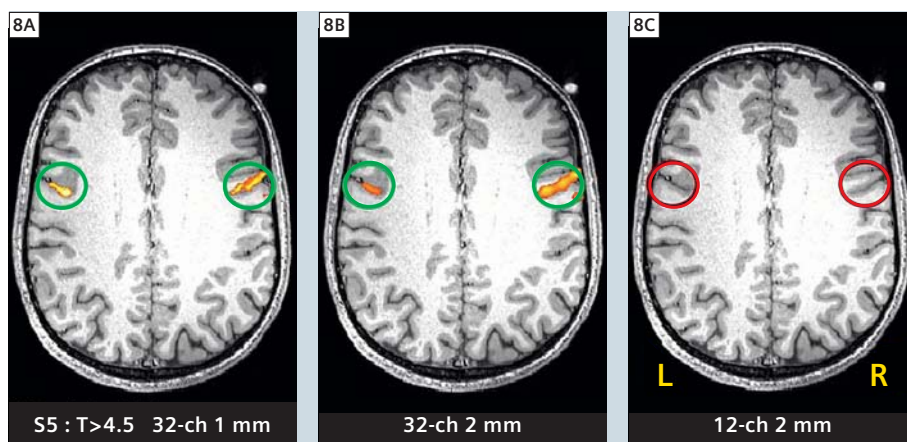
Results

Data from a single subject are shown in Figure 7 illustrating the t-statistics derived from contrast B; complex sequences compared to simple syllables. Activity in the anterior bank of the pre-central sulcus is found in all three acquisitions (1 mm isotropic 32-channels, 2 mm isotropic 32-channels and 2 mm isotropic 12-channels), however the 32-channel coil showed significantly greater sensitivity to the task than the 12-channel Head Matrix coil. Figure 8 demonstrates data from a different individual where activation with 12-channel coil was not detected compared to the 32-channel coil that exhibited activation patterns even at higher resolution (1 mm isotropic).

In this functional MRI study we show that the higher sensitivity of the 32-channel array translates directly into improved detection capability for detecting speech motor activation in individual subjects. Using a high-resolution EPI protocol with the 32-channel coil, we were able to demonstrate sulcal bank specific localization of speech motor activity related to the production of complex sequences of syllables. The amount of required smoothing was limited to the minimum, thus preventing extensive smearing of activity across sulcal banks, bringing the location of the significant voxels to an accurate correspondence with the brain gray matter as identified in the high resolution MPRAGE. This was a significant improvement in localization compared to conventional 3 mm isotropic resolution scans coupled with 6 mm smoothing. In conclusion, our findings demonstrate that employing high-resolution acquisition and highly parallel detection, it is possible to achieve accurate individual-specific mapping of cognitive task related brain networks and enables the examination of individual variability of the structure-function relationship.



7 Activation map (t-statistics) of a single subject overlaid on the 0.6 mm isotropic T1-weighted structural scan. Data acquired with the 12-channel coil are shown at the far right (2 mm isotropic), while 32-channel data are shown at the center (2 mm isotropic) and on the left (1 mm isotropic). Direct comparison of the BOLD activity exhibits higher significance with the 32-channel compared to 12-channel data. Red and yellow indicate lower and higher significance, respectively (FDR = 0.05). (Figure courtesy of S. Ghosh, MIT.)



8 Activation map (t-statistics) from another subject, overlaid on the 0.6 mm isotropic T1-weighted structural scan. Activation is present on the 32-channel data, (A) and (B) green circles, while no activation was detected when using the 12-channel coil (C), red circles. (Figure courtesy of S. Ghosh, MIT.)

b) High-resolution fMRI using a 32-channel coil to improve the accuracy of visual field mapping

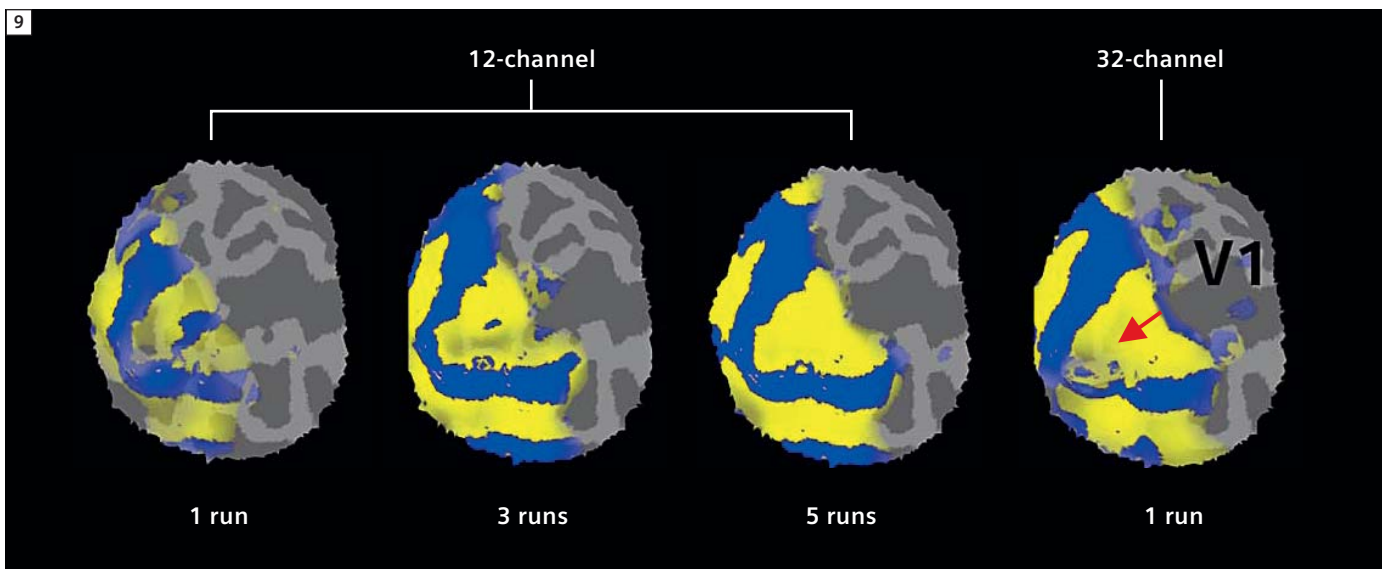
The visual cortex consists of distinct histologically and functionally defined areas arranged topographically based on visual space. Thus, there is a direct topographic mapping of the visual field onto the cortical surface which can be used to identify the boundaries of these areas. This orderly representation is likely to play a critical role in how people process visual information, but it is also often used as a functional marker to locate primary and secondary visual areas in individual subjects as a first step in an fMRI experiment. The mapping of functional boundaries allows a better understanding of the relationships between activation in more complex visual processing experiments. It is important that this initial survey of occipital cortex is robustly and quickly accomplished in each individual subject, so that the bulk of the examination can be devoted to further studies of the workings of the visual system.

In this study we evaluate the potential benefit of highly parallel detectors on the accuracy of fMRI-based mapping of the visual cortex. The visual field mapping benchmark was chosen because the neural organization of primary visual cortex is well understood yet its exact mapping is routinely needed. Furthermore, this benchmark assesses the effect of the array on a more complex fMRI analysis; the quality of boundary estimation is even further dissociated from a simple metric such as image SNR than the more direct measure of activation statistics explored above. Our findings demonstrate that using the 32-channel array provides almost a four-fold decrease in acquisition time needed for a robust estimate of the boundary between visual cortical areas V1 and V2 compared to the 12-channel coil.

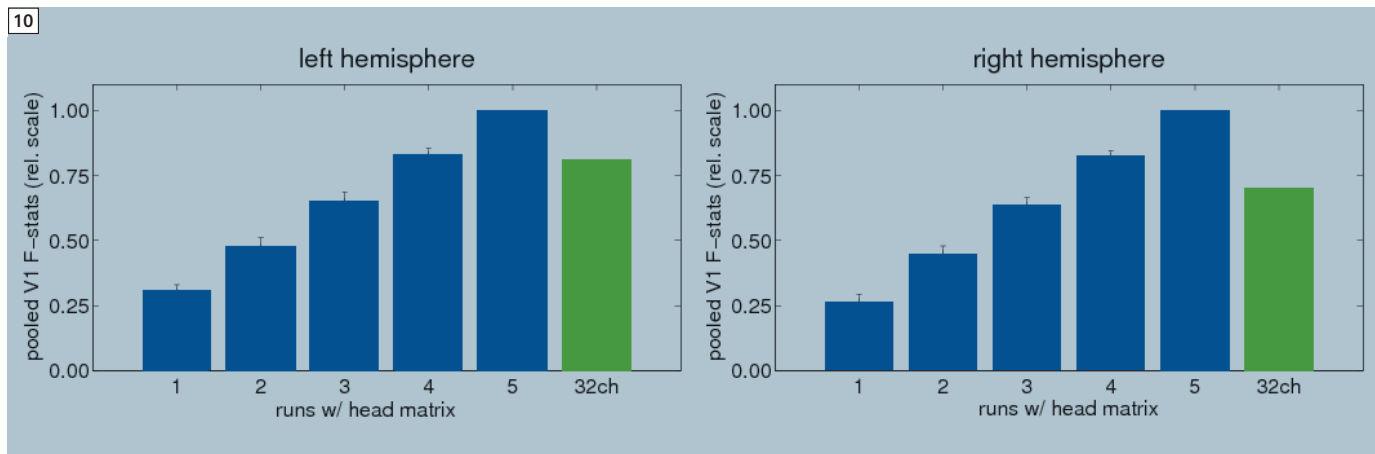
Methods

Data from the two healthy subjects were acquired using the product 12-channel and 32-channel head coils (i.e. each subject was scanned twice). Written consent was obtained from all the sub-

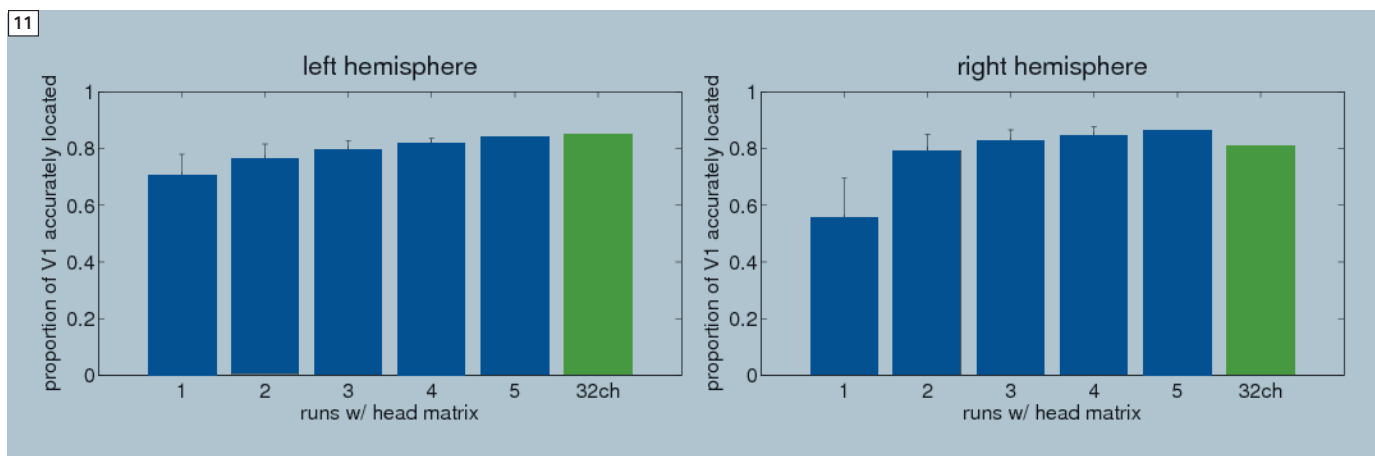
jects under protocols approved by institutional review. Functional MRI data acquired using a single-shot gradient echo EPI sequence. Imaging parameters were: TR = 2000 ms, TE = 30 ms, flip angle = 90°, twenty-eight 2 mm thick slices with inter-slice gap of 0.2 mm and an in-plane resolution of 2 x 2 mm² with FOV = 192 x 192 and matrix = 96 x 96. A high resolution T1-weighted structural scan was acquired using an MPRAGE pulse sequence (voxel size of 1 x 1 x 1 mm³, TR/TI/TE/flip angle = 2530 ms / 1100 ms / 3.48 ms / 7°) and used for slice prescription and to generate the cortical surface for flattened representation of the visual activation. The visual field was mapped using a standard fMRI-based phase-encoded retinotopy paradigm consisting of flickering expanding and contracting rings and clockwise and counterclockwise rotating wedges presented in runs lasting 8 minutes each. A single functional run performed with the 32-channel coil was compared to the average of up to five runs acquired with the 12-channel Head Matrix coil. The visual field representation for each



9 Qualitative comparison in the accuracy of visual field mapping for both 32-channel and 12-channel coils. The same flattened patch of the occipital lobe (left hemisphere in an individual subject) is shown with the field-sign computed from different number of scans and different coils. The color (yellow or blue) indicates the handedness of the local coordinate system of the visual field mapping, while the opacity of the color indicates significance of the fit of the measured BOLD signal to the expected response to the visual stimulus. The single acquisition cycle acquired with the 32-channel coil qualitatively shows a similar V1 detection quality to between 3 and 5 acquisitions with the 12-channel Head Matrix coil. (Figure courtesy of O. Hinds, MIT.)



10 Comparison of the accuracy of V1 identification in both hemispheres, using different numbers of runs with the 2 coils (blue = 12-channels, green = 32-channels). The boundary of V1 was traced on the cortical surface based on the field-sign estimate computed from all data. The total number of correct and incorrect field-sign surface vertices within this region was counted to compute the fraction of V1 depicting the correct field-sign (y axis) for all combinations of a given number of runs (x axis) and for the single run collected with the 32-channel coil. (Figure courtesy of O. Hinds, MIT.)



11 Comparison of the significance (F statistic) of the estimate of the visual field mapping experiment within V1 over different numbers of runs with the 2 coils (blue = 12-channels, green = 32-channels). (Figure courtesy of O. Hinds, MIT.)

functional voxel was determined from the preferred phase of the periodic visual stimulus as estimated using the FSFAST software package. The visual field coordinates were then projected onto the cortical surface generated using the FREESURFER software package [8]. The functional areas, such

as primary visual cortex (V1) and secondary visual cortex (V2), are determined by the handedness of the coordinate system required for the mapping between the visual field and the cortex. Because this handedness is opposite in V1 and V2, it can be used to determine the V1/V2 boundary. Thus, mathemati-

cally, the boundary is determined by a change in the sign of the determinant of the Jacobian of the visual field mapping transformation (a measure of the handedness of its coordinate system referred to as a field-sign reversal).

Results

Figure 9 shows representative field-sign estimates derived from different numbers of runs with the 12-channel coil compared with a single run acquired with the 32-channel coil. V1 is the large yellow region in the center and V2 surrounds V1 in blue. The opacity of the color overlay codes the statistical significance of the result. Qualitatively, a single run with the 32-channel coil has similar accuracy and significance to three runs with the 12-channel array. Figures 10 and 11 show more quantitative results for the accuracy of V1 identification. Figure 10 shows the proportion of cortical surface locations within V1 for which the field-sign was estimated correctly, where “correct” was determined from the average of all the data. The total number of correct and incorrect field-sign locations within this region was counted to compute the fraction of correct assignments for all combinations of runs and coils. Figure 11 shows statistical significance (F-statistic) of the V1 activation for the 2 coils and number of runs. The mean significance of all locations within V1 was computed as a measure of the effective contrast-to-noise ratio of the activation for each coil and given number of runs. This analysis suggests that for retinotopic mapping, a single run with the 32-channel array has the F-statistic significance (proportional to BOLD contrast-to-noise ratio) of between 3 and 4 runs with the 12-channel array.

In this study we compared the 32-channel phased array head coil with the 12-channel Head Matrix coil based on qualitative inspection of the visual field map and quantitative measures of the V1 accuracy and significance of the visual coordinate mapping. Our findings demonstrate that images acquired in a single run using the 32-channel coil provide the same quality retinotopy maps and boundary estimation of V1/V2 areas as three to four acquisitions with the 12-channel coil. A single 8 min stimuli cycle with the 32-channel coil has similar contrast-to-noise ratio within primary visual cortex (V1) as three to four cycles with the 12-channel Head Matrix coil. This is a

greater difference than expected based on the time-series SNR studies above where the tSNR difference at a similar image resolution was about 30%. The greater benefit might result from the difficulty of averaging runs in fMRI; a further inducement to develop technology to achieve the desired activation mapping in as few runs as possible.

Conclusion

Highly parallel detection of functional imaging time-series provides the potential for higher image signal-to-noise ratio (SNR_0) as well as decreased susceptibility distortions in echo-planar imaging. When the time-series is thermal (image) noise dominated, we expect the same general increases in functional contrast-to-noise ratio as seen in imaging comparisons. However, for all but the highest fMRI resolutions, physiological noise becomes increasingly important as SNR_0 is improved, and improvements in image sensitivity from more advanced RF detectors are expected to play a smaller role. Nonetheless, switching to the 32-channel coil improved the tSNR for all of the resolutions and provided clear benefits in the functional experiments.

Acknowledgements

The authors would like to acknowledge Satrajit Ghosh (MIT) and Oliver Hinds (MIT) whose work is included in this manuscript. We thank Steven Shannon and Sheeba Arnold at the A.A. Martinos Imaging Center at MIT, for technical support. We also thank Franz Hebrank, Karsten Jahns, Josef Pfeuffer from Siemens. Special thanks to Michael Hamm for his ongoing support in this collaboration with Siemens.

We acknowledge grant support from the NIDCD (R01 DC01925), NIH (P41RR14075, R01EB007942), and funding from A.A. Martinos Imaging Center at MIT, the McGovern Institute for Brain Research, and Harvard-MIT Health Science and Technology (HST), and a research agreement and research support from Siemens Healthcare. One of us (LLW) acknowledges consulting income from Siemens Healthcare.

References

- 1 Wald LL; Wiggins G. Highly Parallel Detection for MRI. *MAGNETOM Flash* 1/2008, 34–44.
- 2 Wiggins GC, Triantafyllou C, Potthast A, Reykowski A, Nittka M, Wald LL., 32-channel 3 Tesla receive-only phased-array head coil with soccerball element geometry (2006). *Magn Reson Med.*, Vol. 56(1):216–23.
- 3 Krüger G, Glover GH., Physiological noise in oxygenation-sensitive magnetic resonance imaging (2001). *Magn Reson Med.*, Vol. 46(4):631–7.
- 4 Triantafyllou C, Hoge RD, Krüger G, Wiggins CJ, Potthast A, Wiggins GC, Wald LL., Comparison of physiological noise at 1.5 T, 3 T and 7 T and optimization of fMRI acquisition parameters (2005). *NeuroImage*, Vol. 26(1):243–50.
- 5 Kellman P, McVeigh ER., Image reconstruction in SNR units: a general method for SNR measurement (2005). *Magn Reson Med.*, Vol. 54(6): 1439–47.
- 6 Bohland, J.W., and Guenther F.H., An fMRI investigation of syllable sequence production (2006). *NeuroImage*, Vol. 32(2):821–41.
- 7 Sereno MI, Dale AM, Reppas JB, Kwong KK, Belliveau JW, Brady TJ, Rosen BR, Tootell RB, Borders of multiple visual areas in humans revealed by functional magnetic resonance imaging (1995). *Science*, Vol. 12;268(5212): 889–93.
- 8 Dale AM, Fischl B, and Sereno MI, Cortical surface-based analysis. I. Segmentation and surface reconstruction (1999). *NeuroImage*, Vol. 9(2):179–194.

Contact

Christina Triantafyllou, Ph. D.
Massachusetts Institute of Technology
77 Massachusetts Avenue
Cambridge, MA 02139-4307
USA
ctrianta@mit.edu